Rock and Soil Mechanics

Volume 44 | Issue 12 Article 8

2-7-2024

Fatigue analysis of jacket foundations for offshore wind turbines

Yue-ming DU
Center for Hypergravity Experimental and Interdisciplinary Research, Zhejiang University, Hangzhou, Zhejiang 310058, China; College of Civil Engineering and Architecture, Zhejiang University, Hangzhou, Zhejiang 310058, China, yueming_du@zju.edu.cn

De-qiong KONG
Center for Hypergravity Experimental and Interdisciplinary Research, Zhejiang University, Hangzhou, Zhejiang 310058, China; College of Civil Engineering and Architecture, Zhejiang University, Hangzhou, Zhejiang 310058, China, deqiong_kong@zju.edu.cn

Si-liu WANG
Center for Hypergravity Experimental and Interdisciplinary Research, Zhejiang University, Hangzhou, Zhejiang 310058, China; College of Civil Engineering and Architecture, Zhejiang University, Hangzhou, Zhejiang 310058, China

Bin ZHU
College of Civil Engineering and Architecture, Zhejiang University, Hangzhou, Zhejiang 310058, China; Institute of Geotechnical Engineering, Zhejiang University, Hangzhou, Zhejiang 310058, China

Fatigue analysis of jacket foundations for offshore wind turbines

Abstract

Jacket foundations are considered as the most promising solution for offshore wind turbines (OWTs), due to its large lateral stiffness and adaptability to different marine environments. Nowadays, the study on jacket foundations mainly focuses on the bearing and deformation behavior, with significantly less attention being paid to their fatigue damage. Besides, the actual pile-soil interaction is always ignored when assessing the fatigue damage or fatigue life of the foundations for OWTs. This paper presents the development of a three-dimensional numerical model of tetrapod piled jacket foundations, with the interaction between the corner piles and the soil being implemented into it. The numerical model is validated against centrifuge tests. Then, a time-domain fatigue analysis method for OWT jacket foundations is proposed. The influences of pile-soil interaction, wind-wave load coupling effect, and lateral loading direction on the fatigue damage of the jacket are examined in detail. Main findings include: (1) Neglecting the pile-soil interaction will yield significant underestimation, i.e., approximately 40%, of the fatigue damage of OWT jackets, and this becomes even more discernible at the lower oblique support joints, exhibiting an underestimation up to 90% in certain scenarios. (2) Wind load plays a dominant role in determining fatigue damage of the jacket, and the proportion of fatigue damage caused by winds is much greater than that caused by waves. (3) The lateral wind-wave loading along the diagonal direction develops a greater displacement of the jacket than that along the orthogonal direction. However, the corresponding fatigue damage is relatively small, about 70% of that along the orthogonal direction.

Keywords

jacket foundation, fatigue analysis, pile-soil interaction, wind-wave coupling

Rock and Soil Mechanics 2023 44(12): 3639−3652 ISSN 1000−7598
https: //doi.org/10.16285/j.rsm.2022.6709 https://rocksoilmech.researchcommons.org/journal/

Fatigue analysis of jacket foundations for offshore wind turbines

DU Yue-ming[1, 2], KONG De-qiong[1, 2], WANG Si-liu[1, 2], ZHU Bin[2, 3]

1. Center for Hypergravity Experimental and Interdisciplinary Research, Zhejiang University, Hangzhou, Zhejiang 310058, China
2. College of Civil Engineering and Architecture, Zhejiang University, Hangzhou, Zhejiang 310058, China
3. Institute of Geotechnical Engineering, Zhejiang University, Hangzhou, Zhejiang 310058, China

Abstract: Jacket foundations are considered as the most promising solution for offshore wind turbines (OWTs), due to its large lateral stiffness and adaptability to different marine environments. Nowadays, the study on jacket foundations mainly focuses on the bearing and deformation behavior, with significantly less attention being paid to their fatigue damage. Besides, the actual pile-soil interaction is always ignored when assessing the fatigue damage or fatigue life of the foundations for OWTs. This paper presents the development of a three-dimensional numerical model of tetrapod piled jacket foundations, with the interaction between the corner piles and the soil being implemented into it. The numerical model is validated against centrifuge tests. Then, a time-domain fatigue analysis method for OWT jacket foundations is proposed. The influences of pile-soil interaction, wind-wave load coupling effect, and lateral loading direction on the fatigue damage of the jacket are examined in detail. Main findings include: (1) Neglecting the pile-soil interaction will yield significant underestimation, i.e., approximately 40%, of the fatigue damage of OWT jackets, and this becomes even more discernible at the lower oblique support joints, exhibiting an underestimation up to 90% in certain scenarios. (2) Wind load plays a dominant role in determining fatigue damage of the jacket, and the proportion of fatigue damage caused by winds is much greater than that caused by waves. (3) The lateral wind-wave loading along the diagonal direction develops a greater displacement of the jacket than that along the orthogonal direction. However, the corresponding fatigue damage is relatively small, about 70% of that along the orthogonal direction.

Keywords: jacket foundation; fatigue analysis; pile-soil interaction; wind-wave coupling

1 Introduction

Offshore wind power generation is one of the most promising forms of power generation in the field of new energy[1]. During the 13th Five-Year Plan period, China's offshore wind power has experienced rapid development, with the cumulative installed capacity nationwide reaching 8.99 million kw[1−2]. However, with the gradual depletion of nearshore resources, it is an inevitable trend for offshore wind power to move from nearshore to deep-sea areas[1, 3]. Compared with the commonly used large-diameter single-pile wind turbine foundation in shallow waters, the jacket foundation is suitable for deeper waters and high-capacity wind turbine units due to its higher overall stiffness and lower environmental loads from waves and currents[4−5]. Therefore, it has become an increasingly preferred choice for more and more offshore wind turbines (OWTs)[6−7].

The operational environment of OWTs is harsh, and the foundation of OWTs is subjected to various extreme cyclic loads over a long term. As a result, the foundation is highly susceptible to fatigue damage[8−10]. For jacket-type turbines located in deeper waters, the above-mentioned situation becomes even more serious. Therefore, to ensure the safe operation of the turbines throughout their service life, it is necessary to conduct fatigue analysis on the turbine foundation[11].

Currently, there are two main categories of fatigue analysis methods for OWTs: time-domain method and frequency-domain method. Compared to the frequency-domain method, the time-domain method is more time-consuming but can fully consider the nonlinear issues of various environmental loads in time and space, and the calculated results are more accurate[12]. Jia[13] used the time-domain fatigue analysis method to analyze the response of jacket structures under wave loads, and simplified working conditions to reduce computation time. Kvittem et al.[14] found that when simulating fatigue analysis for a long period, it is possible to reduce the impact of randomness on fatigue calculations. Du et al.[15] separately used the time-domain method and the frequency-domain method specified by ABS to calculate fatigue damage for a single-pile foundation offshore platform. They found that the fatigue damage calculated using the frequency-domain method was significantly larger, approximately 3.4 times that of the time-domain method. Mohammadi et al.[16] believed that the actual stress amplitude probability distribution differed from the assumption in the frequency-domain method specified by ABS(American Bureau of Shipping), which was only suitable for narrow banded spectra. Tempel[17] also employed two fatigue analysis methods for turbine foundation fatigue analysis and observed different stress spectra from the two methods. Therefore,

Received: 1 November 2022 Accepted: 8 January 2023
This work was supported by the National Natural Science Foundation of China (52071289, 51988101).
First author: DU Yue-ming, male, born in 1999, Master's student, focusing on offshore wind turbine pile-soil interaction. E-mail: yueming_du@zju.edu.cn
Corresponding author: KONG De-qiong, male, born in 1986, PhD, Professor, research interests: marine geotechnical engineering and large deformation numerical simulation. E-mail: deqiong_kong@zju.edu.cn

to accurately assess the fatigue damage of the jacket-type turbine foundation, the time-domain method is adopted for fatigue analysis in this study.

During the fatigue analysis of OWT foundations, to reduce computational complexity and improve efficiency, the pile-soil interaction is often simplified, such as using soil springs, or even neglecting the pile-soil interaction. Qin et al.[18] modeled only six times the pile diameter below the mud surface to investigate the fatigue characteristics of jacket-type OWTs under the combined action of wind and waves. Yamashita et al.[19] simplified the wind turbine structure above the mud surface into a multi-mass point system for fatigue analysis, without considering the structure below the mud surface. Dong et al.[20] used a decoupled analysis method to investigate the fatigue damage of different tubular joints in jacket foundations, without fully considering the nonlinear response caused by pile-soil interaction. Yeter et al.[21] conducted fatigue analysis on a tripod jacket foundation for wind turbines using soil spring elements. Chang and Wang[22] applied fixed support constraints to pile legs when analyzing the fatigue of the jacket foundation for wind turbines, completely ignoring pile-soil interaction.

However, under the long-term effects of cyclic loads such as wind, waves and currents, the pile-soil interface of OWTs undergoes significant cyclic shear action. The soil around the piles experiences irrecoverable plastic strains, and the pile-soil interaction directly threatens the safety and lifespan of OWTs[6]. Abhinav et al.[23] conducted corresponding experimental studies on whether to consider pile-soil interaction and found that the ultimate strength was overestimated without pile-soil interaction. Wu et al.[24] explored the weakening effect of the surrounding clay through the analysis of the overturning bearing capacity of suction foundations in clay. Zhu et al.[25] conducted centrifuge model tests on jacket foundations under horizontal static and cyclic loads, and found a noticeable weakening effect around the pile-soil interface. Yu et al.[26] also observed the cumulative plastic strain of soft clay in centrifuge tests on single piles of different diameters under horizontal loading. Mao et al.[27] investigated the cumulative displacement response of jacket foundations in layered soil under dynamic loads. Li et al.[28] investigated the shear characteristics of the suction foundation-clay interface under different shear rates and found that when the shear rate reached a certain level, the shear stress−displacement relationship exhibited a strain softening trend. Using ABAQUS finite element software, Wen[29] conducted a large number of parametric analyses on jacket foundations, and they found that under horizontal loads, the rotation center of the jacket foundation gradually moved and approached the downwind pile.

This paper, for the first time, presents a detailed modeling of the pile-soil interaction for tetrapod piled jacket foundations and proposes a time-domain fatigue analysis model that fully considers the pile-soil interaction. Through the fatigue analysis model, the effects of pile-soil interaction, the coupling of wind and wave loads, and the lateral loading direction on the fatigue damage of jacket structures are investigated. This research aims to provide insights into the design of jacket foundation turbines.

2 Wind turbine system parameters

In this study, the wind turbine structural model features a rotor radius of 56 m for the wind turbine generator. The hub is positioned 90 m above the average sea level, and the operational water depth of the working area is 20 m. The tower is characterized by a multi-section variable cross-section hollow cylindrical structure, with a bottom diameter of 4.8 m. The tower is a typical tall and dynamically sensitive structure. The dimensions of this model closely resemble those of wind turbines at a wind farm in Guishan, Guangdong. The structural model is illustrated in Fig. 1.

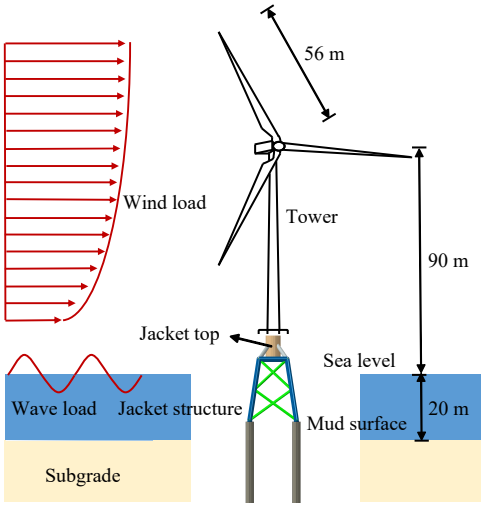

Fig. 1 Schematic diagram of model for jacket-supported offshore wind turbine

3 Numerical model and verification

The finite element model of the tetrapod piled jacket foundation in this study is developed using the commercial finite element software ABAQUS[30]. The model primarily consists of three components: the jacket structure, piles, and soil. This paper mainly focuses on the fatigue damage of the jacket structure considering pile-soil interaction. Therefore, some simplifications are made in modeling the upper structure of the turbine. The overall layout of the finite element model is illustrated in Fig. 2(a).

3.1 Model parameters

The jacket structure is designed to transmit the wind loads born by the upper turbine to the foundation piles. It itself also withstands wave loads and partial wind loads. In this model, the spatial truss elements (T3D2) with a circular tube cross-section are used to model the jacket structure, as depicted in Fig. 2(b). More details regarding the dimensions of the jacket structure are provided in

Table 1. The jacket structure is modeled using elastic materials with the unit weight, elastic modulus, and Poisson's ratio values of 78.5 kN /m³, 206 GPa, and 0.26, respectively.

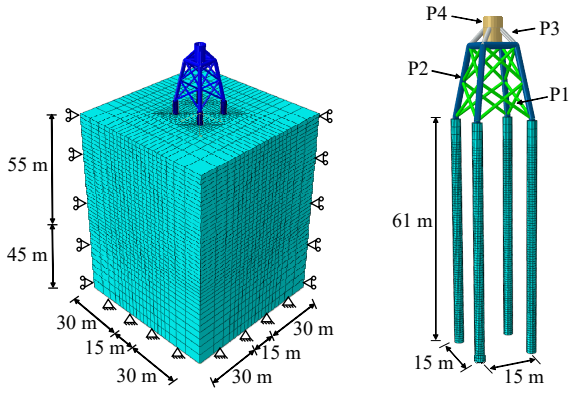

(a) Overall model layout (b) Jacket structure and piles

Fig. 2 Numerical model of the jacket foundation (unit: m)

Table 1 Parameters of jacket trusses in numerical model

No.	Outer diameter /m	Wall thickness /m	Tensile stiffness /MN	Length /m
P1	0.80	0.05	0.81	13.6, 16
P2	1.60	0.15	4.71	17.3
P3	1.20	0.20	6.06	9
P4	4.80	0.25	24.60	7
Pile	2.59	—	4.55	61

The pile foundation is modeled using eight-node linear non-coincident hexahedral elements (C3D8I) to avoid the occurrence of alternating trapezoidal shapes during subsequent meshing, known as the hourglass pattern. The length of the four piles is 61 m, with a diameter of 2.59 m and an embedment depth of 55 m in soil. Piles in ocean engineering are typically hollow steel tubes. The substantial difference in stiffness between hollow steel piles and soft clay poses convergence challenges in numerical calculations. To enhance computational efficiency, the equivalent stiffness method is adopted in this study. Following the principle of equivalent flexural stiffness, solid piles are used instead of hollow piles, and a reduction in density is applied to the model's foundation piles. The piles are modeled using a linear elastic constitutive model, with a mass density of 469.65 kg /m³, an elastic modulus of 13.5 GPa, and a Poisson's ratio of 0.33.

The soil dimensions in Fig. 2(a) are 75 m×75 m× 100 m. The distance between the pile and the boundary is 30 m, which is greater than 10*D*. Therefore, the influence of boundary effects can be ignored to some extent[31]. The selection of parameters for the soil model significantly affects the accuracy of numerical model calculations for the jacket foundation. In this study, the soil is saturated soft clay, modeled using eight-node hexahedral linear reduced integration elements (C3D8R) with an effective unit weight of 6.7 kN /m^3 and a Poisson's ratio of 0.49. The total stress analysis method is employed to simulate undrained conditions. That is, the influence of pore water pressure in the soil is not considered. The stress−strain behavior of the soft clay follows the Tresca yield criterion[32−34]. As illustrated in Fig. 3, the cohesion of the soft clay foundation model linearly increases with the depth, i.e., $S_u = 1.45z$, where z is the depth. The Young's modulus of the soil also linearly increases with the depth[35−36], i.e., $E_s = 500S_u$[37]. In this study, a user subroutine, USDFLD, is developed to implement the linear variation of undrained shear strength and elastic modulus with the depth in soft clay. The USDFLD subroutine is written in Fortran and achieves changes in material properties by redefining field variables at material integration points. This subroutine can obtain real-time location information for each integration point during the analysis computation, and defines this location information as a new field variable. Then, a functional relationship is established in the subroutine between this field variable and state variables (typically material properties related to the solution), thus realizing variations in material properties with the depth[38].

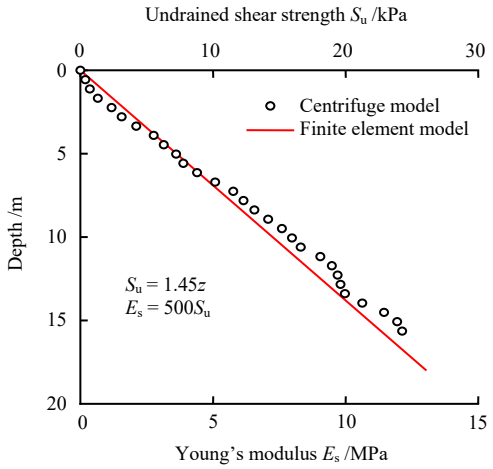

Fig. 3 Distribution of undrained shear strength of clay

3.2 Modeling process

3.2.1 Mesh generation and boundary conditions

As illustrated in Fig. 2(a), to balance computational efficiency and accuracy, a grid refinement technique is applied to the soil around the pile during the mesh generation process[39]. Conversely, for mesh elements located far from the pile and near the ground surface, there is a transition from denser to sparser meshing.

All nodes on the soil lateral boundary surface are constrained in the x and y directions, while all nodes on the bottom boundary of the soil are fully constrained.

3.2.2 Pile-soil contact setting

The correct setting of parameters for the pile-soil contact surface significantly influences the simulation of pile-soil interaction. Zhu et al.[25] observed cracks between piles and soil in centrifuge tests on jacket foundations. Therefore, the model assumed a non-bonded state at the pile-soil

interface that allowed for separation. To more realistically simulate the pile-soil interaction, an "elastic slip deformation" is introduced in the ABAQUS contact settings, which allows a slight relative displacement at the pile-soil contact surface. When defining normal constraint, a hard contact is employed. That is, two objects can transmit normal pressure only in a compressed state, with no restriction on the pressure magnitude. It allows for separation under special conditions.

The Coulomb friction model is employed to simulate the friction at the pile-soil contact surface. Prior to adopting this model, it is necessary to establish contact pairs. In this study, the master-slave surface contact algorithm is utilized. By ensuring a significantly higher stiffness for the master contact surface, better computational accuracy and convergence are achieved. If there is not a substantial difference in stiffness between the two surfaces, the coarser mesh surface is designated as the master surface. In this model, the pile surface serves as the master surface, while the soil contact surface is set as the slave surface. A penalty function is applied to set the tangential properties of the contact surface. The friction coefficient for the contact surface is set to 0.35[38].

3.2.3 Geostress balance

Geotress balance is a necessary step for accurately simulating in-situ stress. In this study, the automatic geostatic stress method is used. By selecting the geostatic automatic incremental step after the initial analysis step, the automatic geostress balance can be achieved. This method is convenient, eliminating the need for importing corresponding initial stress files. In addition, it allows for specifying permissible displacement change tolerances.

3.2.4 Analysis step and loading position

This model includes a total of 4 analysis steps:

Step 1 is the initial analysis step, which mainly involves the application of boundary conditions;

Step 2 is the geostatic stress balance analysis step. During this step, the jacket elements are set to the Model Change state, and the positions of the four pile holes are fixed.

Step 3 is to apply the jacket foundation gravity;

Step 4 involves the application of dynamic loads using the implicit dynamic calculation. In this step, the time history of wind and wave loads on the jacket foundation is input for dynamic computations. The loading application is appropriately simplified. The wind load is simplified as concentrated forces and concentrated moments applied at 1 m from the top of the jacket (31.5 m above the sea level). The wave load is simplified as four concentrated forces applied at four nodes along the middle of the jacket (15.5 m above sea level), as illustrated in Fig. 4(a). Two loading directions are considered in this study: loading along the orthogonal direction and loading along the diagonal direction, as shown in Fig. 4(b).

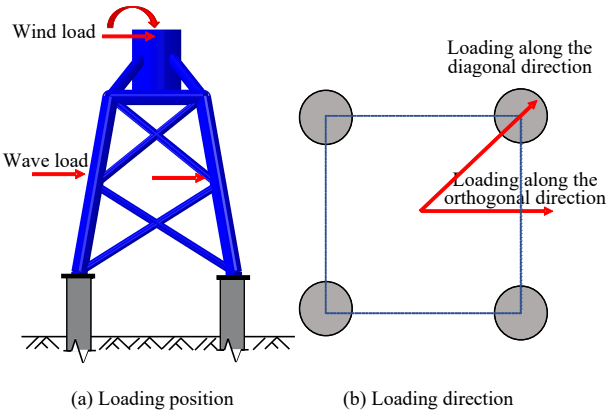

Fig. 4 Loading position and loading direction

3.3 Verification of pile-soil interaction model

To verify the accuracy of the tetrapod piled jacket wind turbine model in simulating pile-soil interaction, centrifuge model tests with unidirectional loading on a tetrapod pile jacket foundation is used as validation tests in this study.

The centrifuge tests are conducted at Zhejiang University on the ZJU-400 geotechnical centrifuge with a centrifugal acceleration of 100*g*. The test foundation soil is soft clay prepared from Malaysian kaolin soil. The undrained shear strength of the saturated soft clay is measured using a T-bar static penetrometer at a penetration rate of 6.0 mm/s. The permeability coefficient of the Malaysian kaolin soil is 2.0×10^{-8} m /s, indicating relatively high permeability, and its consolidation coefficient (C_v) is 40 m^2 /y, approximately equal to 1.27×10^{-2} cm^2 /s. To ensure the undrained condition during the T-bar penetration process, the penetration rate must satisfy $v>20C_v/D$, where D is the diameter of the T-bar probe (5 mm in this case). In this study, the required penetration rate for undrained conditions is approximately 5.08 mm /s. The aforementioned penetration rate satisfies the undrained condition. In addition, a coefficient of 10.5 is employed to relate the penetration resistance during the T-bar penetration process to the undrained shear strength. The measure results are shown in Fig. 3.

In the test, the prototype dimensions of the jacket are consistent with the numerical model. The diameter (D) of the pile is 0.025 9 m, with a wall thickness (d) of 0.002 m. The spacing between adjacent piles (S) is 5.8D. In the jacket model, the pile length is 0.61 m, with 0.065 m above the mud surface and a burial depth of 0.545 m. To measure the displacement response of the loaded structure, LVDTs are installed at both the loading locations and the pile tops. Strain gauges are uniformly placed along the pile to measure the bending moment distribution at different depths and the horizontal displacement at the pile top during the loading process. In post-processing the test results, a sixth-order polynomial is applied to fitting the measured bending moments. The p–y curves are obtained by establishing the interrelationship among pile bending

moments, pile deformations, and soil resistances around the pile.

In this study, the results of load–displacement curves at loading locations, pile deformations, pile bending moment distributions, and *p*–*y* curves obtained from numerical simulations are compared with those from centrifuge model tests, as shown in Fig. 5. The load–displacement curves from both the finite element model and the centrifuge model test exhibit a trend of gradual become gentle with increasing the load. Both demonstrates a work-hardening pattern. Figs. 5(b) and 5(c) illustrate the distribution of pile deformations and pile bending moments along the depth for the front piles (located in front of the loading direction). The maximum pile bending moment has significant guidance for engineering design and, to some extent, reflects the pile-soil interaction. Through comparison, One can see that the maximum pile bending moments occur in the range of 3*D* to 4*D* below the mud surface, and as the load increases, the maximum bending moments tend to move downward. Fig. 5(d) presents a comparison of *p*–*y* curves within the range of 2*D* below the mud surface. It is evident that as the depth increases, both the initial stiffness of the *p*–*y* curve and the ultimate soil resistance around the pile exhibit an increasing trend.

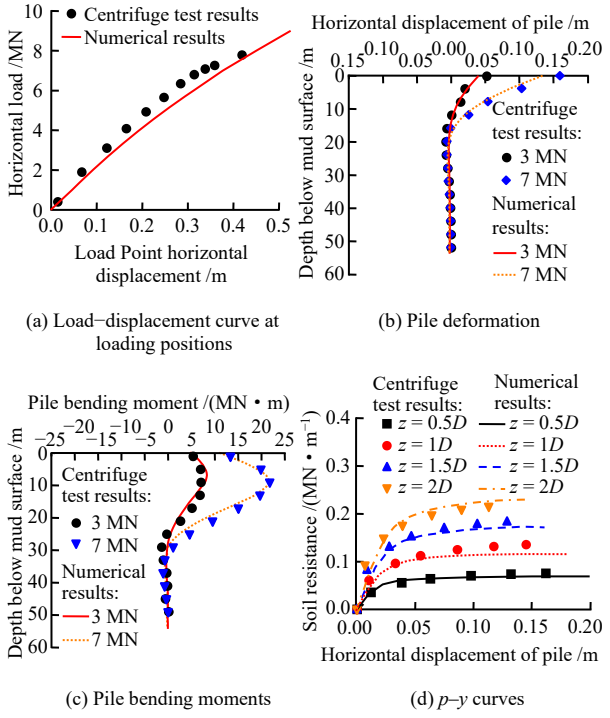

(a) Load–displacement curve at loading positions

(b) Pile deformation

(c) Pile bending moments

(d) *p*–*y* curves

Fig. 5 Comparison of the numerical results with centrifuge data

In general, the numerical model results in this study exhibit good consistency with the centrifuge test results, and the revealed pile-soil interaction patterns of the jacket foundations in soft clay are essentially consistent. Therefore, it is reasonable and reliable to use this numerical model to conduct fatigue analysis of the jacket foundation considering the pile-soil interaction.

4 Environmental load calculation and analysis cases

When conducting dynamic analysis using the time-domain analysis method in this study, the first step involves obtaining the time history of wind and wave loads. Therefore, the time-domain method is used in this paper to calculate wind and wave loads.

4.1 Wind load

4.1.1 Wind speed simulation

To calculate wind loads based on the time-domain method, the first step is to determine the wind speed time history. Then, the wind load time history can be obtained from the wind speed time history. Wind speed is typically composed of fluctuating wind speed and mean wind speed. Mean wind speed can be obtained through on-site observations, and its distribution along the height is generally considered exponential:

$$\frac{\bar{u}(z)}{\bar{u}_{10}}=\left(\frac{z}{10}\right)^{\alpha} \tag{1}$$

where $\bar{u}_{10}$ represents the mean wind speed at the height of 10 m; and α is the surface roughness coefficient, with a value of 0.12 in this study[40].

Fluctuating wind speed is typically assumed to be a zero-mean stationary Gaussian random process time series. The distribution of wind speeds and the interference patterns of different fluctuating wind speeds can be described using power spectral density functions and coherence functions. In this study, the Davenport wind speed spectrum is employed to simulate fluctuating wind speed.

$$S(f)=4w\bar{u}_{10}^{2}\frac{x}{f(1+x^{2})^{2}} \tag{2}$$

where f represents the frequency; w is the bottom roughness coefficient; and $x=1\,200f/\bar{u}_{10}$.

The target spectrum is discretized and then superimposed through the harmonic superposition method. It is essential to ensure the consistency between the resulting spectrum and the target spectrum, and finally the fluctuating wind speed time histories at various heights are obtained. The aforementioned process is implemented using Matlab.

Taking wind case 4 (mean wind speed 14.4 m /s at a height of 10 m above the sea level) as an example, simulations of wind speeds at 45 m and 90 m above the sea level are conducted. The simulation results are shown in Fig. 6, where Fig. 6(a) depicts the time histories of wind speeds in this case. It can be observed that the wind speed exhibits good randomness, consistent with on-site wind speed characteristics. The simulated spectrum is in good agreement with the target spectrum, as shown in Fig. 6(b).

4.1.2 Wind load calculation

Once the wind speeds at different heights are determined, it is necessary to choose an appropriate theory to calculate the wind loads on the wind turbine. In this model, the wind loads are primarily divided into those acting on the top

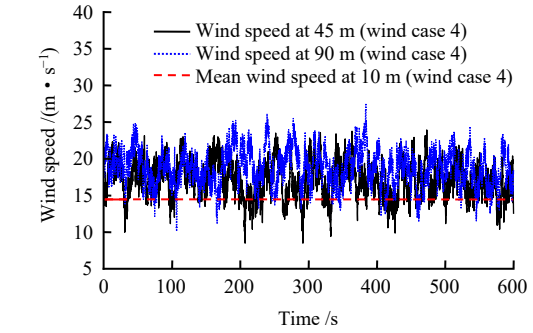

(a) Time histories of wind speeds

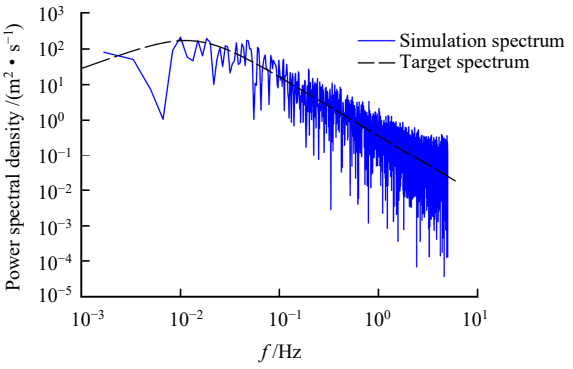

(b) Wind speed simulation spectrum and target spectrum

Fig. 6 Wind speed simulation results

blades and hub, and those acting on the tower. The wind loads on the blades and hub are determined using the thrust coefficient method, and the thrust coefficient is calculated using the blade element momentum theory[40]. For a conservative calculation, only the downwind wind loads are considered in this study.

$$F_{\mathrm{T}} = 0.5 C_{\mathrm{T}} \rho A u^2 \tag{3}$$

where C_{T} is the wind load coefficient; ρ is the air density; A is the swept area of the rotor blades; and u is the instantaneous wind speed.

The wind load on the tower structure is calculated using the following formula:

$$F_{\mathrm{T}} = 0.5 u_{\mathrm{s}} A_{\mathrm{t}} \rho u^2 \tag{4}$$

where u_{s} is the tower shape factor; and A_{t} is the front projection area of the tower. The wind speed simulation results of Section 4.1.1 is presented as an example. The wind load time histories on the wind turbine blades and hub, as well as the tower structure, are shown in Fig. 7.

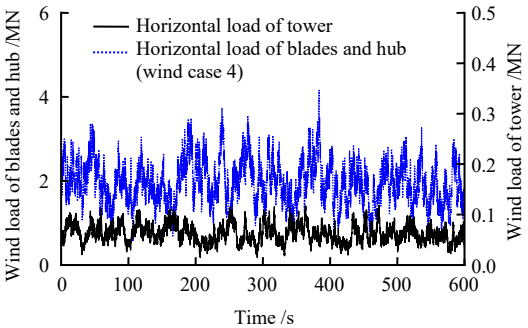

Fig. 7 Time history curves of wind load

4.2 Wave load

4.2.1 Irregular wave simulation

Regarding the simulation of wave loads, Ye et al.[41] accurately reproduced the generation and propagation of waves as well as the seepage of porous media by combining the finite element software ABAQUS with the fluid dynamics software OlaFlow. Yu et al.[42] established a numerical model on the OpenFOAM platform, and used the Open FOAM solver to simulate the nonlinear motion of waves. In this study, to more realistically simulate wave loads with a certain computational efficiency, the irregular wave method is used to simulate real waves. The calculation of wave loads is implemented through Matlab programs. The overall train of thought involves selecting an appropriate wave spectrum and using the linear superposition method to calculate irregular waves. Then, the wave surface height time history curves are obtained. Finally, wave loads are calculated based on the surface height and other wave parameters. The ITTC-modified P-M double-parameter spectrum is chosen to simulate waves, and the wave surface height is obtained through the following equation:

$$\eta(t) = \sum_{i=1}^{m} \sqrt{2 S_{\eta\eta}(\bar{\omega}_1) \Delta\omega_i} \cos(\omega_i t + \varepsilon_i) \tag{5}$$

where $\eta(t)$ is the wave surface height; $S_{\eta\eta}(\omega)$ is the P-M wave energy spectrum density function; m is the number of cosine wave superpositions; and $\Delta\omega_i$ is the frequency spacing.

Wave case 4 (wave height of 3.5 m and period of 8.5 s) is presented as an example, the aforementioned process is implemented using the Matlab program. The wave surface height−time history curve shown in Fig. 8(a). It can be observed that, after the superposition of a series of cosine waves, the entire wave surface height−time series exhibits irregular characteristics. Fig. 8(b) presents a comparison between the simulated wave spectrum and the target spectrum, showing good consistency between the two.

4.2.2 Calculation of wave load

Due to the complexity of the jacket structure, it is impractical to precisely calculate the wave loads acting on it. In this study, when calculating wave loads, the underwater jacket structure is simplified to four steel pipes with diameters identical to the foundation piles. As the pile diameters satisfy the conditions of small-scale cylindrical piles, the Morison formula can be employed to calculate wave loads[12]. The horizontal wave load perpendicular to the circular cylinder can be computed using the following equation:

$$F = F_{\mathrm{D}} + F_{\mathrm{I}} = \frac{1}{2}\frac{\gamma}{g} C_{\mathrm{D}} D_{\mathrm{u}} |u| + \frac{\gamma}{g} C_{\mathrm{M}} A \frac{\partial_{\mathrm{u}}}{\partial_{\mathrm{t}}} \tag{6}$$

$$u = \omega \frac{\mathrm{ch}(kz)}{\mathrm{sh}(kd)} \eta(t) \tag{7}$$

$$\frac{\partial_{\mathrm{u}}}{\partial_{\mathrm{t}}} = \omega^2 \frac{\mathrm{ch}(kz)}{\mathrm{sh}(kd)} \eta(t) \tag{8}$$

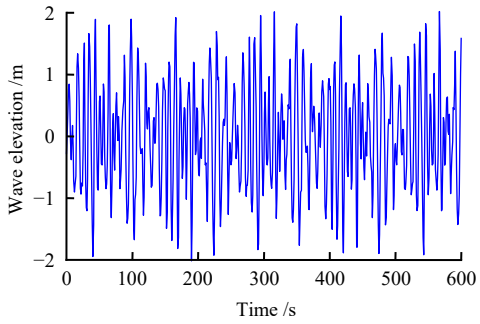

(a) Wave elevation-time history

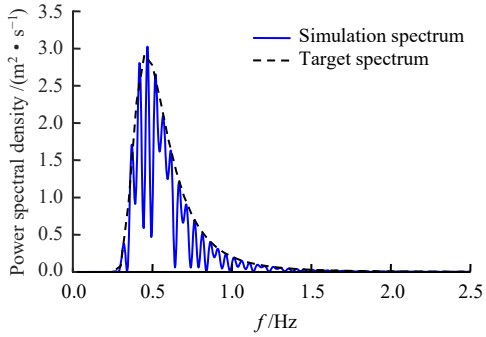

(b) Comparison between simulation and target wave spectra

Fig. 8 Wave simulation results

where D is the diameter of cylindrical pile; F_D is the drag force; F_I is the inertia force; d is the water depth; C_D is drag coefficient; C_M is the inertia coefficient; k is the wave number; and z is the height of the calculation point on the pile.

With the wave simulation results in Section 4.2.1 as an example, the horizontal wave load on a simplified single pile is calculated, as shown in Fig. 9.

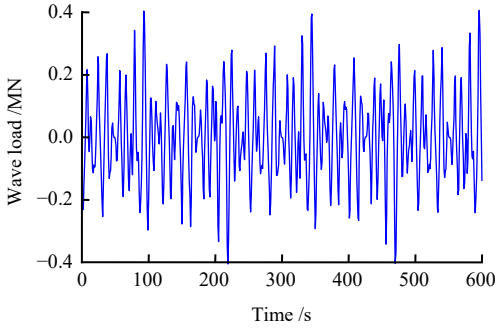

Fig. 9 Time history curve of wave load

4.3 Analysis cases settings

Considering the wave characteristics of the North Atlantic and the typical relationship between wind speed and wave height in typical sea areas around the world, a set of sea conditions, as listed in Table 2, is selected for analysis[12]. Among them, there are six groups each for wind and wave conditions, covering most sea conditions.

A total of six types of fatigue analysis are investigated in this study, including the impact of individual wind and wave actions, wind-wave coupling actions, wind and wave incident directions, and pile-soil interaction on the fatigue life of the jacket structure. Each analysis type includes six specific conditions. The detailed settings for fatigue analysis conditions are shown in Table 3.

Table 2 Division results of wind cases and wave cases

No.	Wind case	Wave case	Probability /%
1	V = 3.244 m /s	H = 0.5 m, T = 5.5 s	5.6
2	V = 7.961 m /s	H = 1.5 m, T = 6.5 s	21.0
3	V = 10.767 m /s	H = 2.5 m, T = 7.5 s	25.9
4	V = 14.452 m /s	H = 3.5 m, T = 8.5 s	26.7
5	V = 17.463 m /s	H = 4.5 m, T = 9.5 s	18.8
6	V = 19.95 m /s	H = 5.5 m, T = 10.5 s	2.0

Note: V is the average wind speed at 10 m above the sea level; H is the significant wave height; and T is the wave period.

Table 3 Arrangement of fatigue analysis cases

No.	Type	Loading direction	Pile-soil interaction	Working condition
A	Wind	Orthogonal	Yes	Wind cases 1−6
B	Wave	Orthogonal	Yes	Wave cases 1−6
C	Wind-wave coupling	Orthogonal	Yes	Cases 1−6
D	Wind-wave coupling	Diagonal	Yes	
E	Wind-wave coupling	Orthogonal	No	
F	Wind-wave coupling	Diagonal	No	

5 Fatigue damage evaluation methods

Based on the previously established finite element model of the tetrapod piled jacket foundation for the offshore wind turbine, the simulation results of wind and wave loads are input into the numerical model for dynamic analysis. Based on the dynamic response results, fatigue analysis is conducted using the full time-domain fatigue analysis method. The overall process of the full time-domain fatigue analysis method is as follows. Firstly, dynamic analysis is performed on the wind turbine structure to obtain the Mises stress time history at key joints of the jacket structure. Then, the rainflow counting method is employed to calculate stress amplitude and stress mean, and to determine the cycle number. The Goodman line[43] is used for mean stress correction. Finally, appropriate S-N curves and fatigue damage theories are selected for computation to obtain the fatigue damage results for the jacket structure.

5.1 Dynamic analysis of finite element model

5.1.1 Natural vibration analysis of jacket structure

When calculating the structural response under cyclic loading, it is generally necessary to analyze the natural frequency of the structure. Yang et al.[44] found that the pile diameter influenced the natural frequencies of the wind turbine system through conducting a natural frequency analysis of a nearshore wind turbine system with a single-pile foundation. Niu[45] conducted a multiple-degree-of-freedom dynamic analysis of a single-pile wind turbine considering pile-soil interaction, and found that the natural frequencies of the wind turbine structure depended on

the pile flexural stiffness, pile diameter, pile embedment depth, soil parameters, height of the wind turbine above the mud surface, and the mass distribution of the wind turbine structure above the mud surface. In this study, solid piles are used instead of hollow piles, but the flexural stiffness of the piles and other influencing factors are kept consistent. It reduces the impact of this treatment on the natural frequencies of the structure.

In the modal analysis of wind turbine structures, it is crucial to consider the overall structure, which includes the tower and transition section. Therefore, in this study, the wind turbine model is improved to include the tower structure when analyzing the natural vibration characteristics. However, it is important to note that due to the significant computational workload involved in full time-domain fatigue analysis, a simplified jacket structure is still utilized to improve computational efficiency.

The results of the natural vibration analysis indicate that the first-order natural frequency of support is 0.348 Hz, the second-order natural frequency is 0.348 Hz, the third-order natural frequency is 2.088 Hz, and the fourth-order natural frequency is 2.091 Hz. The wind rotor speed ranges from 8 to 15.4 r /min, resulting in the first-order natural frequency range of 0.133 to 0.257 Hz, and the third-order natural frequency range of 0.4 to 0.77 Hz. Based on the aforementioned wind turbine natural frequencies, it can be concluded that the first and second natural frequencies of support structure are located between the first and third order natural frequencies of the wind turbine structure, meeting the safety requirements. Additionally, the higher-order natural frequencies are further away from the resonance zone. Therefore, under normal operating conditions, the wind turbine is not affected by resonance frequencies, ensuring its stability and reliability.

5.1.2 Dynamic response of the jacket structure under fatigue load

To determine the drainage pattern of the jacket foundation during cyclic loading, the method recommended by Stewart et al.[46] is used in this study to verify that Case 4, as a representative case, is loaded under the undrained condition.

In this section, Case 4 (wind-wave coupling case) is analysed as an example. The wind and wave loads are input into the finite element model along the orthogonal direction (along the *x*-axis) for a dynamic analysis lasting 600 seconds. The focus of this study is primarily on the fatigue damage to structural joints of the jacket structure. Therefore, the stress on the tower is not considered. The key joint numbers of the jacket structure are shown in Fig. 10. The dynamic response results of the jacket structure are presented in Fig. 11. The Mises stress contour plot of the jacket structure is shown in Fig. 11(a). It reveals that the maximum stress occurs at the bottom part of the tower.

From the stress contour plot, it can be found that the Mises stress is relatively high at Joint K2 (connection between the upper part of the jacket structure and the tower) and Joint K10 (connection between the lower part of the jacket structure and the pile foundation). Moreover, both joints exhibit higher stress in the upwind direction compared to the downwind direction. The Mises stress time histories at Joints K2 and K10 during the 600 seconds are illustrated in Fig. 11(b).

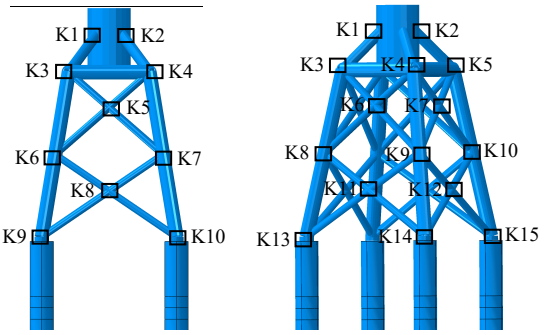

(a) Loading along the orthogonal direction (b) Loading along the diagonal direction

Fig. 10 Joint number of jacket foundation

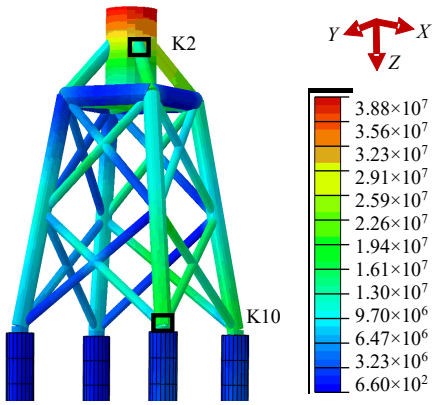

(a) Mises stress of jacket structure

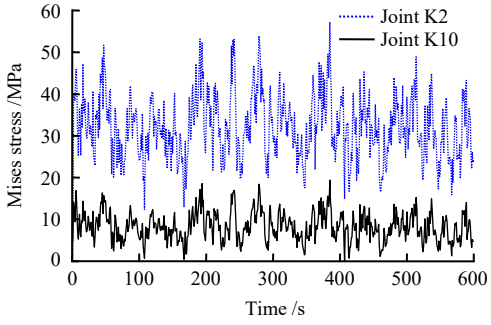

(b) Mises stress time history of joints

Fig. 11 Dynamic response of jacket foundations (Case 4, loading along the orthogonal direction)

5.2 Rainflow counting method

The magnitude of the stress amplitude, the number of cycles, and the mean stress amplitude are crucial parameters influencing the fatigue life of a structure[43]. At present, the rainflow counting method is commonly employed to statistically analyze these parameters. This method counts based on the non-linear stress−strain relationship of the material. That is, a series of closed

stress–strain hysteresis curves are extracted from the random stress response spectrum using the rainflow counting method[47]. This approach comprehensively reflects the entire process of the random load spectrum.

In this study, an improved four-point rainflow counting method is used considering the influence of mean stress on the fatigue life of the structure, and the Goodman line is used to achieve mean stress correction. The aforementioned process is implemented through a Matlab program. To verify the accuracy of the rainflow counting algorithm developed in this study, the results are compared with those obtained by Yeter et al.[21] using the four-point rainflow counting method on the same stress time history curve. The statistical results are completely consistent, with 6 different amplitudes. The number of cycles for each amplitude is 1. This proves the accuracy of the rainflow counting algorithm developed in this study.

With the Mises stress time history data for two key joints reported in Section 5.1.2 as an example, the improved rainflow counting method is applied for statistical analysis. The corresponding results of the mean stress, stress amplitude, and number of cycles are presented in Fig. 12.

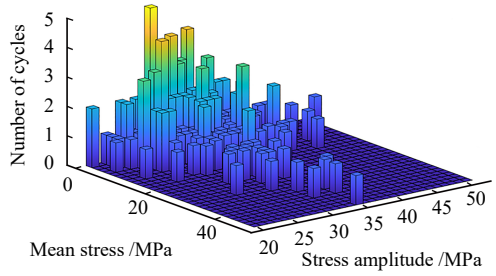

(a) Rainflow counting results of Joint K2

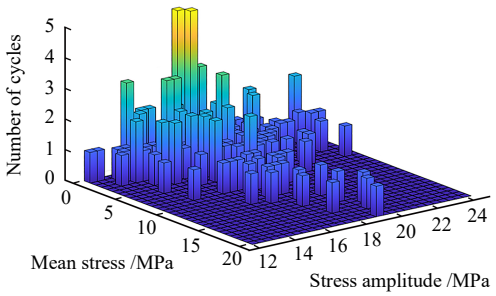

(b) Rainflow counting results of Joint K10

Fig. 12 Statistical results of the rainflow counting method

5.3 S-N curve

The S-N curve is a curve that describes the characteristics of material's fatigue resistance. This curve determines the maximum number of cycles that a material can endure at a specific stress amplitude without fatigue failure[47]. The thickness of the pipe wall also significantly influences the fatigue performance of structural materials. As the wall thickness increases, the fatigue resistance of the pipe joints decreases[43]. As a result, the dual-slope S-N curve provided by DNV[43] regulations is used in this study, which considers the influence of pipe wall thickness:

$$\lg N = \lg \bar{a} - m \lg \left[\Delta\sigma \left(\frac{t}{t_{\text{ref}}} \right)^{k_{\text{t}}} \right] \tag{9}$$

where N is the maximum allowed number of cycles that the structure t_{ref} represents the reference thickness, with a value of 25 mm for non-welded pipe joints, 32 mm for welded pipe joints, and 25 mm for bolts; t is the thickness through which a crack will most likely grow, and $t = t_{\text{ref}}$ is used for thickness less than t_{ref}; and k_{t} is the thickness exponent. The specific parameter values are provided in Table 4.

Table 4 Parameters of S-N curve

Vertical intercept	m	Valid cycle times range	Thickness exponent k_{t}
11.764	3	$N<10^6$	0.2
15.606	5	$N>10^6$	0.2

5.4 Linear fatigue damage theory

Fatigue damage refers to the extent of material damage under fatigue loading, generally denoted by the dimensionless parameter D_{total}. When $D_{\text{total}} = 0$, it indicates that the material has not experienced fatigue damage, and when $D_{\text{total}}>1$, it signifies that the material has reached its fatigue life. Currently, there are roughly two categories of cumulative fatigue damage theories: linear cumulative damage criteria and nonlinear cumulative damage criteria[47]. Due to the complexity of calculations in nonlinear cumulative damage theories and the fact that linear cumulative damage theories can meet engineering precision requirements, linear criteria are mostly used in engineering fatigue analysis. In this study, the P-M linear cumulative fatigue damage theory is primarily employed. The basic formula is as follows:

$$D_{\text{total}} = \sum_i \frac{n_i}{N_i} \tag{10}$$

where N_i represents the maximum allowable number of cycles of the material at the i-th stress amplitude (obtained from the material S-N curve); and n_i is the number of cycles at the i-th stress amplitude (obtained through the rainflow counting method).

Here, the rainflow counting results from Section 5.2 is analysed. The fatigue damage for Joint K2 under the 20-year design life in Case 4 is calculated as 0.199 1, while the fatigue damage for Joint K10 is 0.003 1. The fatigue damage calculated in the following sections is all within a 20-year lifespan.

6 Fatigue damage calculation and result analysis

6.1 Effect of pile-soil interaction on fatigue life

To investigate the impact of pile-soil interaction on fatigue damage of the jacket structure, a fully constrained condition is adopted at the intersection section of the pile-soil surface to neglect pile-soil interaction in this

study. Fatigue analyses are conducted for six cases with and without pile-soil interaction, with the incident direction of wind and waves aligned along the orthogonal direction.

The ratio of fatigue damage for key joints with pile-soil interaction to that without pile-soil interaction is illustrated in Fig. 13. It can be observed that, for Cases 1 and 2 with relatively small wind and wave loads, the impact of pile-soil interaction on fatigue damage of the jacket structure is minor, and the ratio of fatigue damage is close to 1. However, for more extreme wind and wave loads, pile-soil interaction has a significant effect on the fatigue damage of the jacket structure. Neglecting pile-soil interaction would lead to a substantial underestimation of fatigue damage, with an average underestimation of about 40%. It is noteworthy that different joints of the jacket structure exhibit varying sensitivity to pile-soil interaction, with the oblique support joints being the most sensitive.

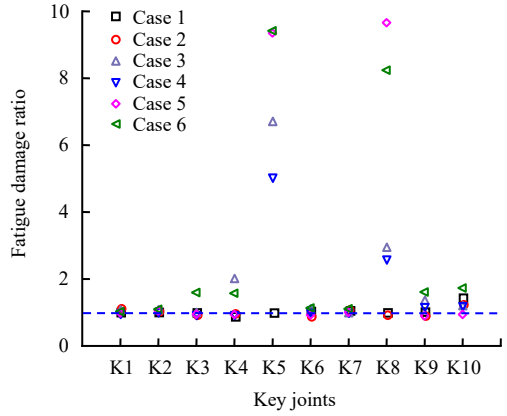

Fig. 13 Fatigue damage ratio at each key joint

6.2 Fatigue under wind and wave loads alone

The fatigue damage values of key joints in the jacket structure under the sole action of wind is illustrated in Fig. 14(a), with a logarithmic scale on the vertical axis for a clearer comparison of fatigue damage values. Six wind cases are analyzed. It reveals significant variations in fatigue damage values among different joints for the same wind condition, with the maximum difference reaching three orders of magnitude, such as Joints K2 and K9 under wind case 2. Under wind loading, the jacket structure's fatigue damage is prone to occur in the upper part. The most dangerous joint is K2, corresponding to the connection between the upper part of the jacket and the tower. In addition, the fatigue damage at downwind joints generally exceeds that at upwind joints at the same height, as observed at Joints K1 and K2, as well as Joints K9 and K10.

The fatigue damage performance of key joints in the jacket structure under the sole action of waves exhibit significant differences compared to that under wind loading alone, as shown in Fig. 14(b). In general, under the same wave condition, the fatigue damage values of various joints in the jacket structure differ more significantly

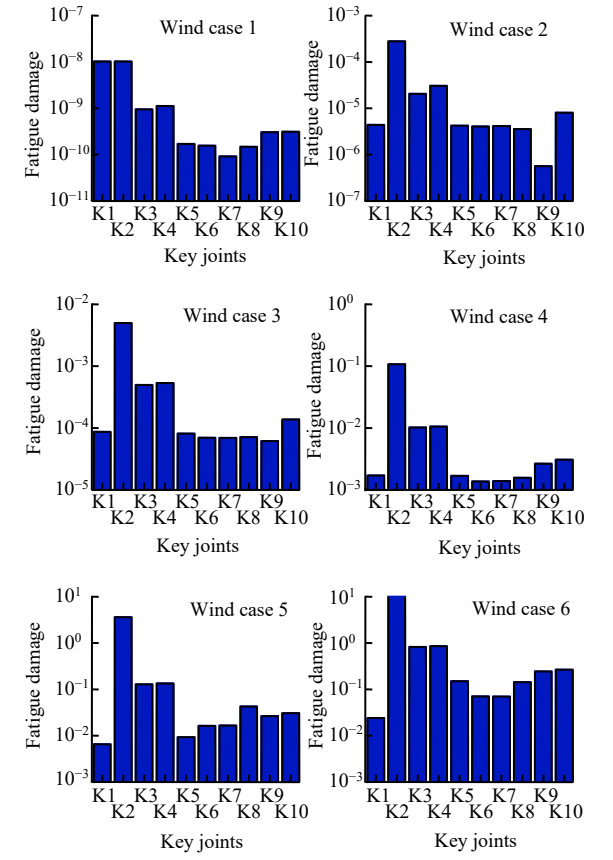

(a) Wind action alone

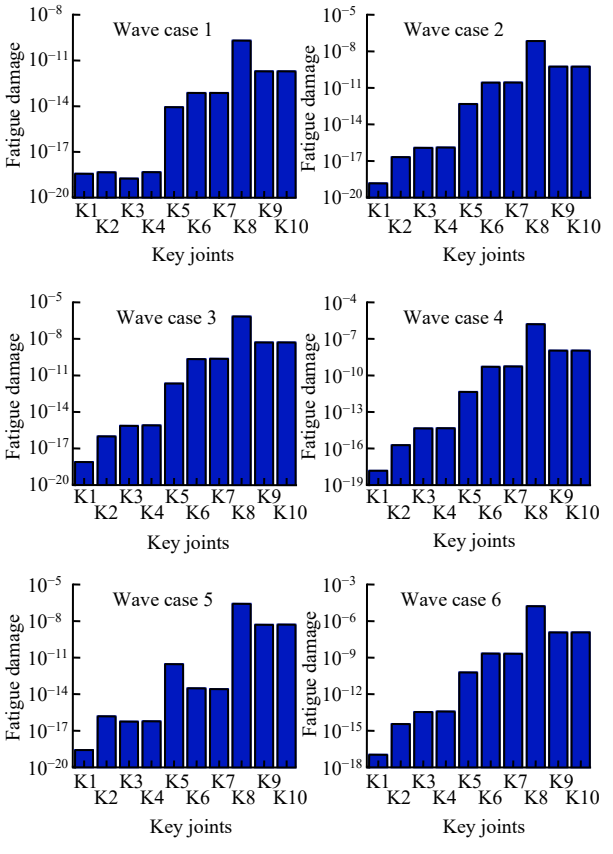

(b) Wave action alone

Fig. 14 Fatigue damage results of key joints under the action of individual wind load and wave load

with the maximum difference reaching 10 orders of magnitude, far exceeding the differences in fatigue damage values under wind loading alone. Wave loading has a greater impact on the fatigue damage in the lower part of the jacket structure, and the most dangerous joint is the lower oblique support joint. Furthermore, there is little difference in fatigue damage among key joints at the same height in the jacket structure, which is different under wind loads. For the six wave cases considered, none of the key joints in the jacket structure reach the fatigue damage failure threshold within a 20-year lifespan. It indicates that they are in a safe state. However, under wind loading alone, the key joints in the jacket structure experience fatigue failure when the average wind speed reaches 17.463 m /s (wind case 5) at 10 m above the sea level.

6.3 Fatigue under wind-wave coupling effect

The fatigue damage values of various key joints in the jacket structure under the wind-wave coupling effect are presented in Fig. 15. Fatigue damage in the jacket structure under the wind-wave coupling effect also tends to occur in the upper part, with the most dangerous joint being K2, consistent with cases of wind load acting alone. It is noteworthy that under the wind-wave coupling effect,

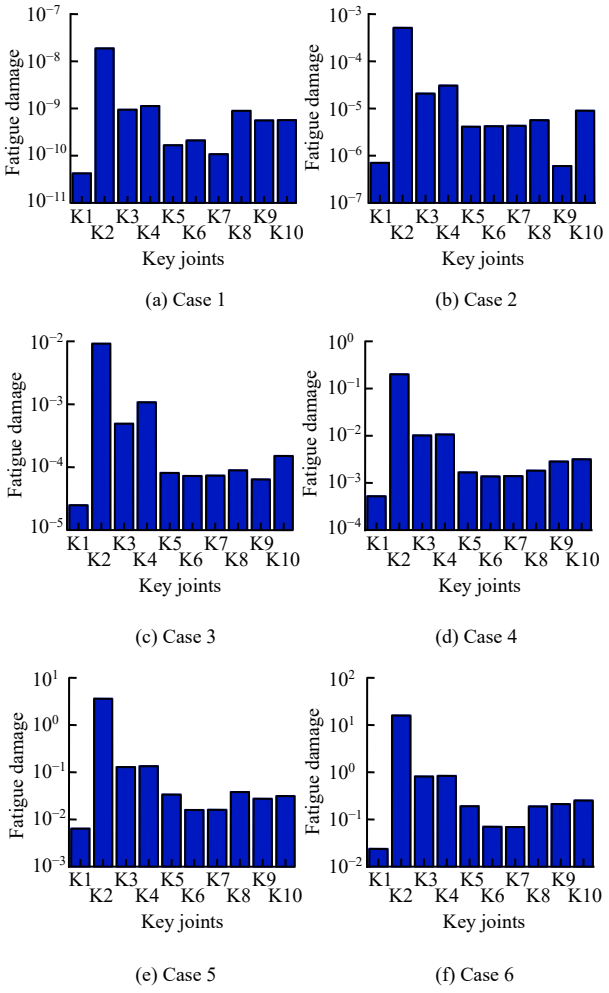

Fig. 15 Fatigue damage results under the action of wind-wave coupling load (along the orthogonal direction)

the fatigue damage in the jacket structure is predominantly caused by wind loads, as shown in Fig. 16. It can be observed that wave-induced fatigue damage is much smaller than wind-induced fatigue damage, and the superposition of waves weakens the fatigue damage in some joints, such as Joint K1. However, overall, the wind-wave coupling effect leads to an increase in fatigue damage.

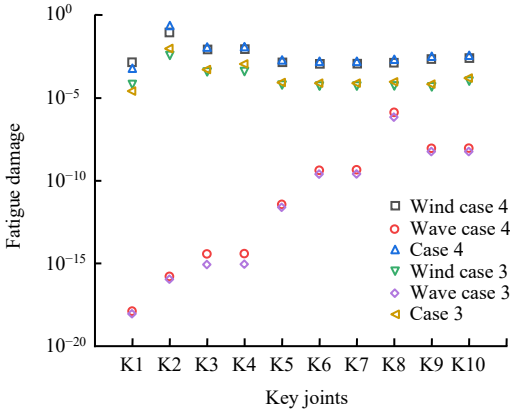

Fig. 16 Influence of wind and wave loads on the fatigue of jacket structure

The horizontal displacement at the pile top of the jacket foundation during the dynamic analysis is illustrated in Fig. 17. It is evident that the wave-induced horizontal displacement at the pile top is relatively small, while the wind load results in larger horizontal displacements. The displacement variations under the wind-wave coupling effect are consistent with those induced by wind alone. It aligns with the dominance of wind load in fatigue analysis of the wind turbine, as shown in Fig. 16. The superposition of wave loads causes the horizontal oscillations induced by wind loads to intensify or weaken at certain periods. Overall, the horizontal displacement oscillations at the pile top under the wind-wave coupling effect are more pronounced. Fig. 18 shows the predicted fatigue life for each key joint based on the occurrence probability of each case. The shortest fatigue life is observed at Joint K3, which is estimated to be 20.7 years (fatigue damage value of 0.966). For conservative estimation, the most dangerous joint is considered as representative of the fatigue life of the jacket structure. Therefore, the fatigue

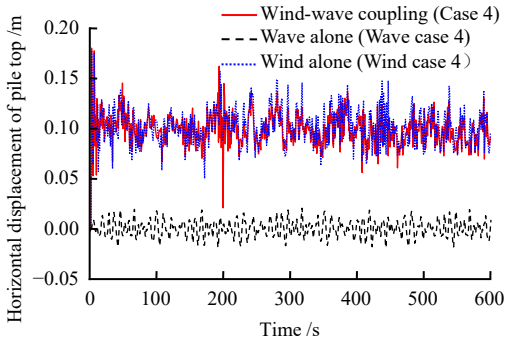

Fig. 17 Horizontal displacement curve of pile top

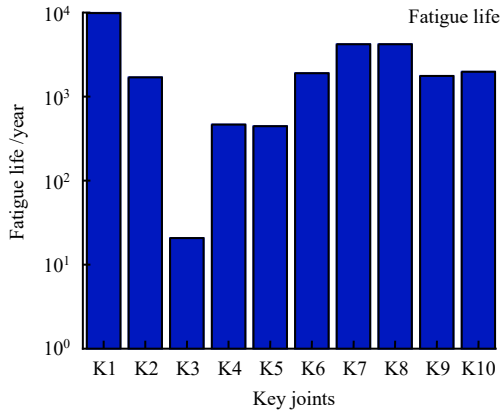

Fig. 18 Prediction of fatigue life

life of the jacket structure of the wind turbine model under combined operating conditions is estimated to be 20.7 years.

6.4 Fatigue life against incident direction of wind and waves

Under actual sea conditions, the wind and wave directions are not fixed. In this study, to investigate the impact of wind and wave incident directions on the fatigue damage of the jacket structure, two extreme incident directions are selected for fatigue analysis: loading along the orthogonal direction and loading along the diagonal direction.

The fatigue damage values of key joints in the jacket structure under wind-wave coupling effect under the diagonal loading are presented in Fig. 19. It can be seen that for the same case, the fatigue damage values of joints on the cross-section perpendicular to the incident direction are relatively small compared to other joints at the same height, such as Joints K4, K9, and K14. When loaded along the diagonal direction, the most dangerous joint in the jacket structure is K5, which differs slightly from the case of loading along the orthogonal direction. Under the both conditions, the most dangerous joint remains located in the upper part of the jacket structure.

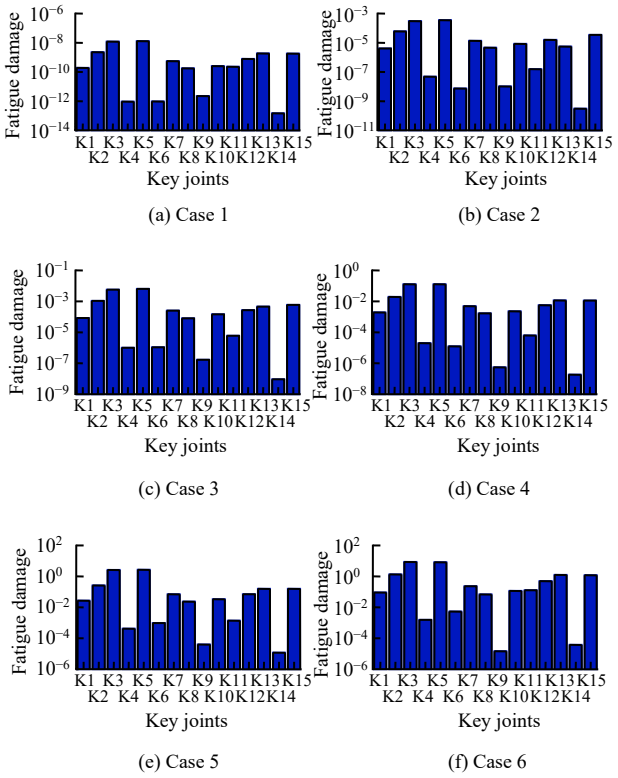

Fig. 19 Fatigue damage results under wind-wave coupling load (along the diagonal direction)

The ratio of fatigue damage values under the diagonal loading to that under the orthogonal loading for each case is illustrated in Fig. 20, where the fatigue damage values are obtained from the most dangerous joint in the structure. It can be observed that the fatigue damage under the diagonal loading is smaller than that under the orthogonal loading, approximately 70% of the damage under orthogonal loading. Therefore, the most dangerous fatigue loading direction is along the orthogonal direction. Fig. 21 presents the horizontal displacement response at the top of the jacket structure under different loading directions for Case 4. It can be seen that the diagonal loading induces larger displacements in the jacket structure, consistent with the observations of centrifuge experiments of Zhu et al.[25]. Consequently, concerning fatigue life, the orthogonal direction is the most dangerous incident direction, while considering the displacement response of the wind turbine, the diagonal direction is deemed the most dangerous incident direction.

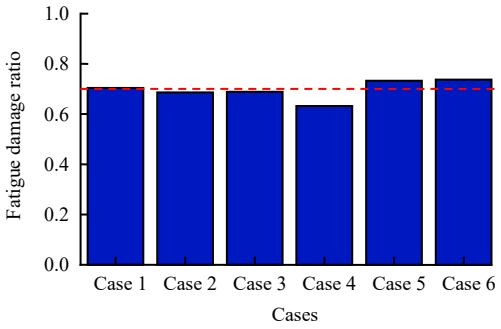

Fig. 20 Ratio of the maximum fatigue damage of loading along the diagonal direction to that of loading along the orthogonal direction

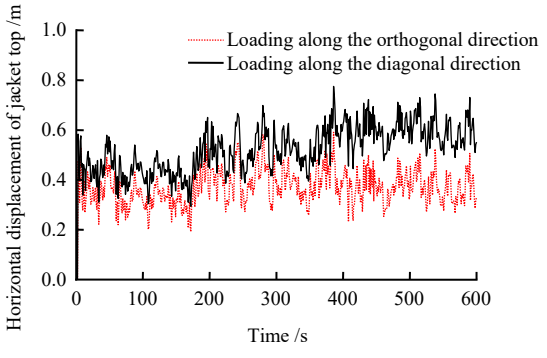

Fig. 21 Horizontal displacement curve of jacket top under different loading directions

7 Conclusions

In this paper, a fatigue analysis model for the tetrapod piled jacket foundation of nearshore wind turbines is proposed for the first time. The nonlinear problems of wind and wave loads in both time and space domains are fully considered. The full time-domain fatigue analysis method is used to investigate the impact of pile-soil interaction, coupling of wind and wave loads, lateral loading direction on the fatigue life of the jacket structure. And the fatigue life is also predicted. The main conclusions can be drawn as follows:

(1) The pile-soil interaction has a significant influence on the fatigue damage of the middle and lower parts of the jacket structure. Neglecting pile-soil interaction could lead to a substantial underestimation (approximately 40%) of fatigue damage in the jacket structure. The impact on fatigue damage is most pronounced for the lower oblique support joints. Neglecting pile-soil interaction may result in a 90% underestimation of fatigue damage at the most dangerous location of the jacket structure in certain scenarios.

(2) Wind loads play a predominant role in the fatigue damage of the jacket structure, far exceeding the influence of wave loads. When subjected to wind loads alone, the most dangerous location for fatigue damage in the jacket structure is at the upper connection between the jacket and the tower. Under wave loads alone, the most dangerous location for fatigue damage is in the lower section of the jacket. In the case of wind-wave coupling, the most dangerous location for fatigue damage in the jacket structure is at the connection between the tower and the jacket, consistent with the scenario of wind loads alone.

(3) When subjected to diagonal loading, the most dangerous location for fatigue damage in the jacket structure differs slightly from that under orthogonal loading, but both remains in the upper section of the jacket. In comparison to orthogonal loading, diagonal loading induces larger displacement responses in the jacket structure, while the associated fatigue damage is relatively smaller, approximately 70% of that under orthogonal loading.

It should be noted that the primary focus of this study is on the issue of fatigue damage in the upper jacket structure of the wind turbine. The linear elastic model of the Tresca yield criterion is a relatively simple constitutive model, and it has limitations in accurately depicting soil softening behaviors[48]. Furthermore, due to the challenges in centrifuge tests for cyclic loading on soft clay in meeting the time scale[49], the results have not been validated using centrifuge test data under cyclic loading. These aforementioned issues are still subject to further investigation.

References

[1] QIN Hai-yan. Review and prospect of offshore wind power development in China[J]. China Academic Journal Electronic Publishing House, 2022, 12(2): 50−58.

[2] ZHENG Yi-yun. The Development status of offshore wind power and the preliminary analysis on the promotion of Shanghai Offshore Wind power project[J]. Shanghai Energy Conservation, 2022(8): 1035−1038.

[3] SEIDEL M. Jacket substructures for the RE power 5M wind turbine[C]//Conference Proceedings European Offshore Wind. [S. l.]: [s. n.], 2007: 1−8.

[4] ABHINAV K A, SAHA N. Stochastic response of jacket supported offshore wind turbines for varying soil parameters[J]. Renewable Energy, 2017, 101(C): 550−564.

[5] ZHU Zhou-jie. Model tests on pile group effect and cyclic effect of jacket foundation of offshore wind turbines[D]. Hangzhou: Zhejiang University, 2017.

[6] ZHOU Wen-jie, WANG Li-zhong, TANG Lü-jun, et al. Numerical analysis of dynamic responses of jacket supported offshore wind turbines[J]. Journal of Zhejiang University (Engineering Science), 2019, 53(8): 1431−1437, 1447.

[7] DONG W, MOAN T, GAO Z. Fatigue reliability analysis of the jacket support structure for offshore wind turbine considering the effect of corrosion and inspection[J]. Reliability Engineering & System Safety, 2012, 106: 11−27.

[8] ASSON P. Damage equivalent wind-wave correlations on basis of damage contour lines for the fatigue design of offshore wind turbines[J]. Renewable Energy, 2015, 81: 723−736.

[9] ZIEGLER L, VOORMEEREN S, SCHAFHIRT S, et al. Design clustering of offshore wind turbines using probabilistic fatigue load estimation[J]. Renewable Energy, 2016, 91(C): 425−433.

[10] DO T Q, LINDT J W V D, MAHMOUD H. Fatigue life fragilities and performance-based design of wind turbine tower base connections[J]. Journal of Structural Engineering, 2015, 141(7): 04014183.

[11] ZHAO Jian-bin, XI Yi-bo, WANG Zhen-yu. Fatigue damage calculation method of monopile supported offshore wind turbine[J]. Journal of Zhejiang University (Engineering Science), 2019, 53(9): 1711−1719.

[12] FAN Hui-yan. Dynamics and fatigue analysis on monopile foundation of offshore wind turbine under wind and wave loads[D]. Harbin: Harbin Institute of Technology, 2016.

[13] JIA J. An efficient nonlinear dynamic approach for calculating wave induced fatigue damage of offshore structures and its industrial applications for lifetime extension[J]. Applied Ocean Research, 2008, 30(3): 189−198.

[14] KVITTEM M I, MOAN T. Time domain analysis procedures for fatigue assessment of a semisubmersible wind turbine[J]. Marine Structures, 2015, 40: 38−59.

[15] DU J, LI H, ZHANG M, et al. A novel hybrid frequency-time domain method for the fatigue damage assessment of offshore structures[J]. Ocean Engineering, 2015, 98: 57−65.

[16] MOHAMMADI S F, GALGOUL N S, STAROSSEKU, et al. An efficient time domain fatigue analysis and its comparison to spectral fatigue assessment for an offshore jacket structure[J]. Marine Structures, 2016, 49: 97−115.

[17] TEMPEL J. Design of support structures for offshore wind turbines[D]. Delft: Delft University of Technology, 2006: 162.

[18] QIN Pei-jiang, MA Yong-liang, HAN Chao-shuai, et al. Frequency-domain fatigue assessment of support structure for offshore wind turbine[J]. Journal of Zhejiang University (Engineering Science), 2017, 51(9): 1712−1719.

[19] YAMASHITA A, SEKITA K. Analysis of the fatigue damage on the offshore wind turbines exposed to wind and wave loads within the typhoon area[C]//ASME 2004, International Conference on Offshore Mechanics and Arctic Engineering. Vancouver: ASME, 2004: 284−291.

[20] DONG W, MOAN T, GAO Z. Long-term fatigue analysis of multi-planar tubular joints for jacket-type offshore wind turbine in time domain[J]. Engineering Structures, 2011, 33(6): 2002−2014.

[21] YETER B, GARBATOV Y, SOARES C G. Fatigue damage assessment of fixed offshore wind turbine tripod support structures[J]. Engineering Structures, 2015, 101: 518−528.

[22] CHANG Ka, WANG Kun-peng. Study on fatigue characteristics of jacket fan structure under combined wind and wave conditions[J]. Renewable Energy Resources, 2021, 39(12): 1617−1622.

[23] ABHINAV K A, SAHA N. Nonlinear dynamical behavior of jacket supported offshore wind turbines in loose sand[J]. Marine Structures, 2018, 57: 133−151.

[24] WU Y Q, YANG Q, LI D Y, et al. Limit equilibrium solutions to anti-overturning bearing capacity of suction caissons in uniform and linearly increasing strength clays[J]. Canadian Geotechnical Journal, 2022, 59(2): 304−313.

[25] ZHU B, YING P P, ZHU Z, et al. Centrifuge modelling of lateral cyclic behaviour of a tetrapod piled jacket in soft clay[J]. Proceedings of the Institution of Civil Engineers-Geotechnical Engineering, 2021, 174(1): 44−57.

[26] YU Jan, HUANG Mao-song, ZHANG Chen-rong. Model tests and analysis of single piles with two different diameters subjected to cyclic lateral loadings in clay[J]. Rock and Soil Mechanics, 2016, 37(4): 973−980.

[27] MAO D F, ZHONG C, ZHANG L, et al. Dynamic response of offshore jacket platform including foundation degradation under cyclic loadings[J]. Ocean Engineering, 2015, 100: 35−45.

[28] LI Da-yong, ZHANG Yu-kun, GAO Yu-feng, et al. Shear behavior of suction foundation-clay interface under different shear rates[J]. Journal of Disaster Prevention and Mitigation Engineering, 2022, 42(1): 231−236.

[29] WEN Kai. Numerical modelling on tetrapod piled jacket foundations for offshore wind turbines subject to lateral monotonic and cyclic loads[D]. Hangzhou: Zhejiang University, 2019.

[30] SYSTÉMES DASSAULT. Abaqus Analysis users' Manual[M]. Providence, RI, USA: Simula Corparation, 2013.

[31] CHAUDHRY A R. Static pile-soil-pile interaction in offshore pile groups[D]. Oxford: University of Oxford, 1994.

[32] FAYYAZI M S, TAIEBAT M, FINN W D L. Group reduction factors for analysis of laterally loaded pile groups[J]. Canadian Geotechnical Journal, 2014, 51(7): 758−769.

[33] GEORGIADIS K. Variation of limiting lateral soil pressure with depth for pile rows in clay[J]. Computers and Geotechnics, 2014, 62: 164−174.

[34] MIAO L F, GOH A T C, WONG K S, et al. Three-dimensional finite element analyses of passive pile behaviour[J]. International Journal for Numerical and Analytical Methods in Geomechanics, 2006, 30(7): 599−613.

[35] ZHU S, CHEN R, KANG X. Centrifuge modelling of a tetrapod jacket foundation under lateral cyclic and monotonic loading in soft soil[J]. Canadian Geotechnical Journal, 2021, 58(5): 637−649.

[36] LIU R, LIU M, TIAN Y, et al. Effect of perforations on the bearing capacity of shallow foundation on clay[J]. Canadian Geotechnical Journal, 2019, 56(5): 746−752.

[37] COMODROMOS E M, PAPADOPOULOU M C. Response evaluation of horizontally loaded pile groups in clayey soils[J]. Géotechnique, 2012, 62(4): 329−339.

[38] ZHU B, WEN K, KONG D, et al. A numerical study on the lateral loading behaviour of offshore tetrapod piled jacket foundations in clay[J]. Applied Ocean Research, 2018, 75: 165−177.

[39] WEN K, WU X , ZHU B. Numerical investigation on the lateral loading behaviour of tetrapod piled jacket foundations in medium dense sand[J]. Applied Ocean Research, 2020, 100: 102193.

[40] Ministry of Housing and Urban-Rural Development of the People's Republic of China. GB 5009−2012 Load code for the design of building structures[S]. Beijing: China Architecture & Building Press, 2012.

[41] YE J H, YU D. ABAQUS-OlaFlow integrated numerical model for fluid-seabed-structure interaction[J]. Marine Structures, 2021, 78: 103016.

[42] YU Xiu-xia, LI Xin, LING Xian-chang, et al. Seabed liquefaction around offshore wind turbine pipe pile foundation under nonlinear wave load[J]. Journal of Engineering Geology, 2021, 29(5): 1599−1610.

[43] Det Norske Veritas. DNV-RP-C203 Fatigue design of offshore steel structure[S]. Norway: Det Norske Verital, 2006.

[44] YANG Chun-bao, WANG Rui, ZHANG Jian-min. Numerical method for calculating system fundamental frequencies of offshore wind turbines with monopile foundations[J]. Engineering Mechanics, 2018, 35(4): 219−225.

[45] NIU Wen-jie, Numerical method for calculating system fundamental frequencies of offshore wind turbines with monopile foundations[J]. China Earthquake Engineering Journal, 2016, 38(5): 713−719.

[46] STEWART D P, RANDOLPH M F. A new site investigation tool for the centrifuge[C]//Proceedings of International Conference Centrifuge. Rotterdam, the Netherlands: A. A. Balkema, 1991.

[47] SUN Ze-li. Research of fatigue limit capacity of jacket offshore wind turbine using fully coupled analysis method[D]. Dalian: Dalian University of Technology, 2021.

[48] JIAO Yu-qi, HE Lin-lin, LIANG Yue, et al. Study of vertical bearing capacity of spudcan foundations considering strain-softening effect of structured clay[J]. Rock and Soil Mechanics, 2022, 43(5): 1374−1382.

[49] TAYLOR R N. Geotechnical centrifuge technology[M]. [S. l.]: [s. n.], 1995.